

# NLO QCD corrections to $W^+W^-b\bar{b}$ production at hadron colliders

A. Denner,<sup>1</sup> S. Dittmaier,<sup>2</sup> S. Kallweit,<sup>3</sup> and S. Pozzorini<sup>4</sup>

<sup>1</sup>*Universität Würzburg, Institut für Theoretische Physik und Astrophysik, 97074 Würzburg, Germany*

<sup>2</sup>*Albert-Ludwigs-Universität Freiburg, Physikalisches Institut, 79104 Freiburg, Germany*

<sup>3</sup>*Paul Scherrer Institut, Würenlingen und Villigen, 5232 Villigen PSI, Switzerland*

<sup>4</sup>*Institut für Theoretische Physik, Universität Zürich, 8057 Zürich, Switzerland*

(Dated: June 22, 2011)

Top-antitop quark pairs belong to the most abundantly produced and precisely measurable heavy-particle signatures at hadron colliders and allow for crucial tests of the Standard Model and new-physics searches. Here we report on the calculation of the next-to-leading order (NLO) QCD corrections to hadronic  $W^+W^-b\bar{b}$  production, which provides a complete NLO description of the production of top-antitop pairs and their subsequent decay into W bosons and bottom quarks, including interferences, off-shell effects, and non-resonant backgrounds. Numerical predictions for the Tevatron and the LHC are presented.

PACS numbers: 12.38.Bx, 12.38.Cy, 13.85.-t, 14.65.Ha

The top quark is the heaviest of all known elementary particles and is expected to play a key role in any theory of the flavour sector of elementary particles. Its precise investigation is, thus, of great importance at the current hadron colliders Tevatron and LHC, where top quarks are mostly produced via top-antitop ( $t\bar{t}$ ) pairs.

The first step towards precise theoretical predictions for  $t\bar{t}$  production at hadron colliders was made already about 20 years ago with the calculation of QCD corrections at next-to-leading-order (NLO) [1–4]. Later also electroweak radiative corrections were calculated [5–9], and recently important progress has been achieved both in the resummation of logarithmically enhanced terms [10–13] and towards the inclusion of QCD corrections at next-to-next-to-leading-order [14–24].

The above-mentioned predictions are based on the approximation of stable (on-shell) top quarks, i.e. the top-quark decays, which proceed into pairs of W bosons and b quarks in the Standard Model, were ignored. Recently also studies [25–27] at the NLO QCD level have been presented that include the top-quark decays via a spin-correlated narrow-width approximation, i.e. the top quarks are still on shell. In this letter we present first results<sup>1</sup> at NLO QCD on the further generalization that the intermediate top quarks can be off their mass shell, i.e. we consider the process of  $W^+W^-b\bar{b}$  production, including leptonic W-boson decays.

The reaction  $pp \rightarrow W^+W^-b\bar{b} + X$  represents one of the few remaining  $2 \rightarrow 4$  LHC background processes on the Les Houches wishlist [28]. While various such  $2 \rightarrow 4$  NLO QCD calculations have been performed in the recent years (see e.g. Ref. [28] for a review),  $W^+W^-b\bar{b}$

production involves the treatment of resonant particles for the first time in a hadron-collider environment on that level of complexity. The two resonances can be consistently treated in the complex-mass scheme that was introduced at the NLO level in the context of the calculation of the electroweak corrections to the processes  $e^+e^- \rightarrow WW \rightarrow 4 \text{ fermions}$  [29, 30], which was the first full NLO calculation for a  $2 \rightarrow 4$  particle process.

At leading order (LO), hadronic  $W^+W^-b\bar{b}$  production proceeds via partonic channels with quark-antiquark ( $q\bar{q}$ ) and gluon-gluon ( $gg$ ) initial states. A few representative diagrams are depicted in Fig. 1. In addition to doubly-resonant (DR) diagrams, where the  $W^+W^-b\bar{b}$  final state results from the decay of a  $t\bar{t}$  pair, our calculation also includes singly-resonant and non-resonant contributions. As is well known, the bulk of the inclusive  $W^+W^-b\bar{b}$  cross section is efficiently reproduced by the widely used narrow-width approximation, which incorporates all DR effects in the limit of vanishing top-quark width,  $\Gamma_t \rightarrow 0$ . By including all off-shell effects from doubly-, singly-, and non-resonant diagrams, our calculation consistently describes all contributions that are suppressed by one or more powers of  $\Gamma_t/m_t$ . These extra terms are mandatory in order to achieve percent-level precision in the (inclusive and differential) description of  $t\bar{t}$  production, and for a reliable simulation of off-shell  $W^+W^-b\bar{b}$  final states. To describe top-quark decays in a realistic way we also include the leptonic W-boson decays  $W^+ \rightarrow \nu_e e^+$  and  $W^- \rightarrow \bar{\nu}_\mu \mu^-$  in a spin-correlated narrow-width approximation.

In the following we briefly sketch the calculation of the virtual and real corrections. A more detailed description will be presented elsewhere. In order to prove the correctness of our results we have evaluated each ingredient twice and independently. The treatment of the virtual QCD corrections to  $q\bar{q}/gg \rightarrow W^+W^-b\bar{b}$  is based on diagrammatic representations of the one-loop amplitudes and numerical reduction of tensor integrals [31, 32]. The

<sup>1</sup> Similar results on  $WWbb$  production have recently been shown by the HELAC-OPP collaboration at the meeting of the HEPTOOLS network at Granada (see <http://indico.cern.ch/conferenceDisplay.py?confId=91923>).

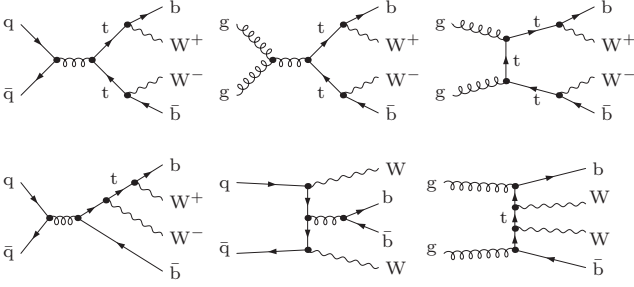


FIG. 1: Representative LO diagrams of doubly-resonant (upper line), singly-resonant (first diagram in lower line), and non-resonant type (last two diagrams in lower line).

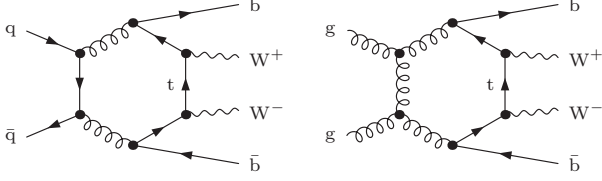


FIG. 2: Hexagon diagrams in  $q\bar{q}/gg \rightarrow W^+W^-b\bar{b}$ .

$q\bar{q}$  and  $gg$  channels comprise about 300 and 800 one-loop diagrams, respectively. The most complicated ones are the 84 pentagons and 21 hexagons that contribute to the  $gg$  channel (see examples in Fig. 2) and involve tensor integrals up to rank five. Feynman diagrams are generated with two independent versions of FEYNARTS [33, 34], and one-loop amplitudes are reduced along the lines of Refs. [35, 36] using two in-house MATHEMATICA programs, one of which relies on FORMCALC [37] for preliminary manipulations. The employed approach strongly mitigates the complexity inherent in Feynman diagrams by exploiting factorisation of colour matrices, reduction of helicity structures to compact spinor chains, and recycling of a multitude of common subexpressions. The treatment of rational terms of ultraviolet or infrared origin is described in Appendix A of Ref. [35]. The reduced expressions are automatically converted into FORTRAN77 programs that evaluate colour/helicity summed quantities with very high CPU efficiency. Tensor integrals are related to scalar integrals by means of numerical algorithms that avoid instabilities from inverse Gram determinants and other spurious singularities [31, 32].

The presence of intermediate unstable top quarks in  $pp \rightarrow W^+W^-b\bar{b} + X$  represents a non-trivial new aspect as compared to previous NLO QCD studies of multi-particle processes. To regularise intermediate top-quark resonances in a gauge-invariant way we employ the complex-mass scheme [30]. In this approach the top-quark width  $\Gamma_t$  is incorporated into the definition of the renormalised (squared) top-quark mass,  $\mu_t^2 = m_t^2 - im_t\Gamma_t$ . In the on-shell scheme this complex parameter  $\mu_t^2$  is identified with the position of the pole of the top-quark prop-

agator, and the top mass counterterm  $\delta\mu_t$  is related to the top-quark self-energy at  $p_t^2 = \mu_t^2$  via (see (4.25) in Ref. [30])

$$\delta\mu_t = \frac{\mu_t}{2} [\Sigma^{t,R}(\mu_t^2) + \Sigma^{t,L}(\mu_t^2) + 2\Sigma^{t,S}(\mu_t^2)]. \quad (1)$$

We note that an expansion of the occurring self-energies around the real point  $p_t^2 = m_t^2$  (as e.g. suggested in (4.27) in Ref. [30]) is not sufficient for NLO accuracy, because the top-quark self-energy is not analytic at the complex pole,  $p_t^2 = \mu_t^2$ . The evaluation of one-loop scalar box integrals in presence of complex masses represents another non-trivial aspect of the complex-mass scheme. In our calculation we employ the results of Ref. [38], where explicit analytic continuations have been presented for all kinematic box configurations that are relevant for physical processes.

The real corrections receive contributions from the  $2 \rightarrow 5$  partonic processes  $gg \rightarrow W^+W^-b\bar{b}g$  and  $q\bar{q} \rightarrow W^+W^-b\bar{b}g$ , as well as from crossing-related  $gq$  and  $g\bar{q}$  channels. The  $2 \rightarrow 5$  matrix elements are evaluated with MADGRAPH [39] and, alternatively, using the Weyl-vander-Waerden formalism of Ref. [40]. To isolate infrared divergences and cancel them analytically we employ in-house implementations of the dipole subtraction formalism [41]. Specifically this is done in dimensional regularization with strictly massless light quarks (including b quarks) and alternatively in a hybrid scheme with small quark masses with the respective dipole subtraction terms from Ref. [42].

Colour and helicity correlations that enter the subtraction procedure are generated by means of AUTODIPOLE [43] and, alternatively, in analytic form. To achieve sufficient numerical stability we perform the 11-dimensional phase-space integration using multi-channel Monte Carlo techniques with weight optimisation [44]. The integration of the dipole-subtracted  $2 \rightarrow 5$  contributions is optimised by means of additional channels corresponding to the dipole kinematics.

In the following we present predictions for the Tevatron ( $p\bar{p}$  collisions at 1.96 TeV) and the LHC ( $pp$  collisions at 7 TeV). In NLO(LO) QCD we employ MSTW2008NLO(LO) parton distributions [45] and describe the running of the strong coupling constant  $\alpha_s$  with two-loop(one-loop) accuracy, including five active flavours. Contributions induced by the strongly suppressed bottom-quark density are neglected. For the gauge-boson and top-quark masses we use  $m_t = 172$  GeV,  $M_W = 80.399$  GeV, and  $M_Z = 91.1876$  GeV. The masses of all other quarks, including b quarks, are neglected. In view of the negligibly small Higgs-mass dependence we adopt the  $M_H \rightarrow \infty$  limit, i.e. we omit diagrams involving Higgs bosons. The electroweak couplings are derived from the Fermi constant  $G_\mu = 1.16637 \times 10^{-5} \text{ GeV}^{-2}$  in the  $G_\mu$ -scheme, where the sine of the mixing angle and the electromagnetic coupling read  $s_w^2 = 1 - M_W^2/M_Z^2$  and

$\alpha = \sqrt{2}G_\mu M_W^2 s_w^2/\pi$ . For consistency, we perform the LO and NLO calculations using the top-quark widths  $\Gamma_{t,\text{LO}} = 1.4655 \text{ GeV}$  and  $\Gamma_{t,\text{NLO}} = 1.3376 \text{ GeV}$  [46], respectively. Since the leptonic W-boson decay does not receive NLO QCD corrections we employ the NLO W-boson width  $\Gamma_W = 2.0997 \text{ GeV}$  everywhere. Final-state quarks and gluons with pseudo-rapidity  $|\eta| < 5$  are converted into infrared-safe jets using the anti- $k_T$  algorithm [47]. For the Tevatron (LHC) we set the jet-algorithm parameter  $R = 0.4$  (0.5) and apply the transverse-momentum and pseudo-rapidity cuts  $p_{T,b\text{-jet}} > 20$  (30) GeV,  $|\eta_{b\text{-jet}}| < 2.5$ . Moreover, we require a missing transverse momentum of  $p_{T,\text{miss}} > 25$  (20) GeV and charged leptons with  $p_{T,l} > 20 \text{ GeV}$  and  $|\eta_l| < 2.5$ .

The LO and NLO  $W^+W^-b\bar{b}$  cross sections at the Tevatron and at the LHC are plotted in Fig. 3 as a function of the renormalisation and factorisation scales,  $\mu_{\text{ren}} = \mu_{\text{fact}} = \mu$ . At the Tevatron, where the cross section is dominated by the  $q\bar{q}$  channel, at  $\mu = m_t$  we obtain  $\sigma_{\text{LO}}^{\text{Tev}} = 44.31_{-12.49}^{+19.68} \text{ fb}$  and  $\sigma_{\text{NLO}}^{\text{Tev}} = 41.75_{-3.79}^{+0.00} \text{ fb}$ , where the uncertainties describe missing higher-order corrections estimated via scale variations in the range  $m_t/2 < \mu < 2m_t$ . For the LHC, where the gg channel dominates, we obtain  $\sigma_{\text{LO}}^{\text{LHC}} = 662.4_{-174.1}^{+263.4} \text{ fb}$  and  $\sigma_{\text{NLO}}^{\text{LHC}} = 840_{-75}^{+27} \text{ fb}$ . Normalising the results to LO predictions at  $\mu = m_t$  we obtain the relative NLO corrections  $K^{\text{Tev}} = 0.942_{-0.085}^{+0.000}$  and  $K^{\text{LHC}} = 1.27_{-0.11}^{+0.04}$ . The NLO corrections induce a moderate shift of the integrated cross section and reduce its scale uncertainty from about 44% (40%) to 9% (9%) at the Tevatron (LHC). This confirms the good convergence of perturbative predictions at the scale  $\mu = m_t$ , a feature that is reflected also in the stable shape of the NLO curves in Fig. 3.

To assess the impact of finite-width effects on the integrated cross section we have extrapolated our numerical results to the narrow-width limit  $\Gamma_t \rightarrow 0$ . In this region we observe a linear  $\Gamma_t$ -dependence, consistent with the cancellation of logarithmic soft-gluon singularities. At the Tevatron we find that finite-width effects shift the LO(NLO) cross section by about  $-0.8\%$  ( $-0.9\%$ ). At the LHC we observe a qualitatively different behaviour: the shift induced by finite-width contributions is smaller in size and positive. At LO it amounts to  $+0.4\%$ , and at NLO it becomes as small as the Monte Carlo statistical error ( $+0.2\%$ ).

To illustrate NLO and finite-width corrections to differential observables, in Fig. 4 we plot the invariant-mass distribution of a positron and a b-jet—the visible products of a top-quark decay—at the Tevatron. In narrow-width and LO approximation this kinematic quantity is characterised by a sharp upper bound,  $M_{e+b}^2 \leq m_t^2 - M_W^2$ , which renders it very sensitive to the top-quark mass. The value of  $m_t$  can be extracted with high precision using, for instance, the invariant-mass distribution of a positron and a  $J/\psi$  from a  $B$ -meson

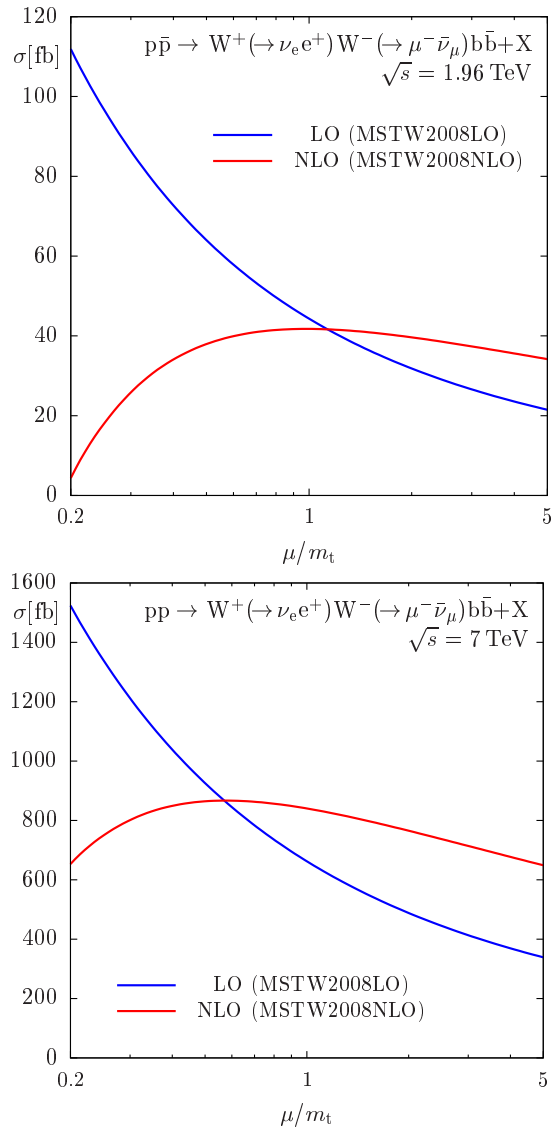


FIG. 3: Scale dependence of the LO and NLO  $W^+W^-b\bar{b}$  cross sections at the Tevatron and the LHC.

decay [48], an observable that is closely related to  $M_{e+b}$ . In Fig. 4 we clearly see, already in LO, small but non-negligible off-shell contributions that elude the kinematic bound. At NLO this feature becomes more pronounced, also due to QCD radiation that enters the b-jet without being emitted from its parent b quark. Below the kinematic bound we find very significant NLO effects. In the region  $50 \text{ GeV} < M_{e+b} < 150 \text{ GeV}$  the shape of  $M_{e+b}$  is strongly distorted, with corrections ranging from  $+15\%$  to  $-30\%$  (see lower plot). In the vicinity of the kinematic bound the NLO prediction is barely consistent with the LO uncertainty band. This example demonstrates the importance of  $2 \rightarrow 4$  NLO predictions for a precise description of the kinematic details of the  $W^+W^-b\bar{b}$  final state and, more generally, for the top-physics programme at the Tevatron and at the LHC.

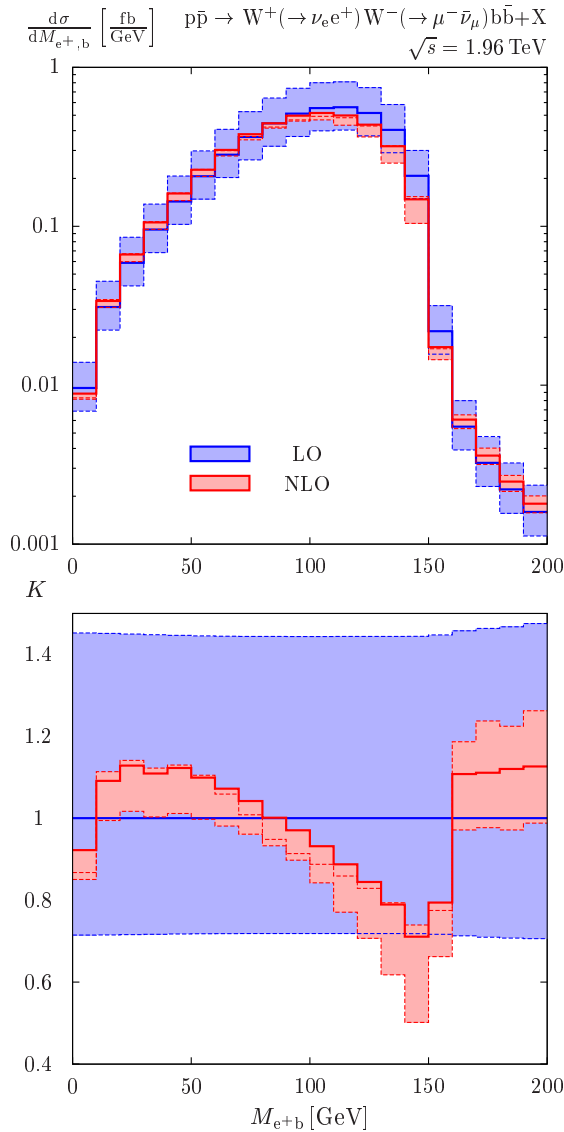


FIG. 4: Invariant mass  $M_{e+b}$  of the positron-b-jet system at the Tevatron: absolute LO and NLO predictions (upper plot) and relative corrections w.r.t. LO at  $\mu = m_t$  (lower plot). The uncertainty bands describe  $m_t/2 < \mu < 2m_t$  variations.

S.P. thanks the Swiss National Science Foundation for support. This work is supported in part by the European Community's Marie-Curie Research Training Network HEPTOOLS under contract MRTN-CT-2006-035505.

Note added: Shortly after the submission of this paper results of a similar calculation by the HELAC-OPP Collaboration have been published in Ref. [49].

[1] P. Nason et al., Nucl. Phys. **B327**, 49 (1989).  
[2] W. Beenakker et al., Nucl. Phys. **B351**, 507 (1991).  
[3] M. L. Mangano, P. Nason, and G. Ridolfi, Nucl. Phys. **B373**, 295 (1992).

[4] S. Frixione et al., Phys. Lett. **B351**, 555 (1995).  
[5] W. Beenakker et al., Nucl. Phys. **B411**, 343 (1994).  
[6] S. Moretti, M. R. Nolten, and D. A. Ross, Phys. Lett. **B639**, 513 (2006).  
[7] J. H. Kühn, A. Scharf, and P. Uwer, Eur. Phys. J. **C51**, 37 (2007).  
[8] W. Bernreuther, M. Fückler, and Z.-G. Si, Phys. Rev. **D74**, 113005 (2006), hep-ph/0610334.  
[9] W. Bernreuther, M. Fückler, and Z.-G. Si, Nuovo Cim. **B123**, 1036 (2008).  
[10] M. Beneke, P. Falgari, and C. Schwinn, Nucl. Phys. **B828**, 69 (2010), 0907.1443.  
[11] M. Czakon, A. Mitov, and G. F. Sterman, Phys. Rev. **D80**, 074017 (2009), 0907.1790.  
[12] V. Ahrens et al., JHEP **1009**, 097 (2010), 1003.5827.  
[13] N. Kidonakis, Phys. Rev. **D82**, 114030 (2010), 1009.4935.  
[14] S. Dittmaier, P. Uwer, and S. Weinzierl, Phys. Rev. Lett. **98**, 262002 (2007), hep-ph/0703120.  
[15] B. Kniesl et al., Phys. Rev. **D78**, 094013 (2008).  
[16] C. Anastasiou and S. M. Aybat, Phys. Rev. **D78**, 114006 (2008).  
[17] M. Czakon, A. Mitov, and S. Moch, Phys. Lett. **B651**, 147 (2007).  
[18] M. Czakon, A. Mitov, and S. Moch, Nucl. Phys. **B798**, 210 (2008).  
[19] M. Czakon, Phys. Lett. **B664**, 307 (2008).  
[20] R. Bonciani et al., JHEP **07**, 129 (2008).  
[21] R. Bonciani et al., JHEP **0908**, 067 (2009), 0906.3671.  
[22] R. Bonciani et al. (2010), 1011.6661.  
[23] A. Gehrmann-De Ridder and M. Ritzmann, JHEP **0907**, 041 (2009), 0904.3297.  
[24] M. Czakon, Phys. Lett. **B693**, 259 (2010), 1005.0274.  
[25] W. Bernreuther et al., Nucl. Phys. **B690**, 81 (2004), hep-ph/0403035.  
[26] K. Melnikov and M. Schulze, JHEP **08**, 049 (2009).  
[27] W. Bernreuther and Z.-G. Si, Nucl. Phys. **B837**, 90 (2010).  
[28] J. R. Andersen et al. (SM and NLO Multileg Working Group) (2010), 1003.1241.  
[29] A. Denner et al., Phys. Lett. **B612**, 223 (2005).  
[30] A. Denner et al., Nucl. Phys. **B724**, 247 (2005).  
[31] A. Denner and S. Dittmaier, Nucl. Phys. **B658**, 175 (2003).  
[32] A. Denner and S. Dittmaier, Nucl. Phys. **B734**, 62 (2006).  
[33] J. Küblbeck, M. Böhm, and A. Denner, Comput. Phys. Commun. **60**, 165 (1990).  
[34] T. Hahn, Comput. Phys. Commun. **140**, 418 (2001).  
[35] A. Bredenstein et al., JHEP **08**, 108 (2008).  
[36] A. Bredenstein et al., JHEP **1003**, 021 (2010).  
[37] T. Hahn and M. Perez-Victoria, Comput. Phys. Commun. **118**, 153 (1999).  
[38] A. Denner and S. Dittmaier, Nucl. Phys. **B844**, 199 (2011).  
[39] J. Alwall et al., JHEP **09**, 028 (2007).  
[40] S. Dittmaier, Phys. Rev. **D59**, 016007 (1999).  
[41] S. Catani and M. H. Seymour, Nucl. Phys. **B485**, 291 (1997).  
[42] S. Catani et al., Nucl. Phys. **B627**, 189 (2002).  
[43] K. Hasegawa, S. Moch, and P. Uwer, Comput. Phys. Commun. **181**, 1802 (2010).  
[44] R. Kleiss and R. Pittau, Comput. Phys. Commun. **83**, 141 (1994).  
[45] A. D. Martin et al., Eur. Phys. J. **C63**, 189 (2009).

- [46] M. Jezabek and J. H. Kühn, Nucl. Phys. **B314**, 1 (1989).
- [47] M. Cacciari, G. P. Salam, and G. Soyez, JHEP **04**, 063 (2008).
- [48] A. Kharchilava, Phys. Lett. **B476**, 73 (2000).
- [49] G. Bevilacqua et al. (2010), 1012.4230.